

Cover Page



Universiteit Leiden



The handle <http://hdl.handle.net/1887/20094> holds various files of this Leiden University dissertation.

Author: Melis, Joost

Title: Nucleotide excision repair in aging and cancer

Date: 2012-11-06



Chapter 2

Chapter 2

Life-spanning murine gene expression profiles in relation to chronological and pathological aging in multiple organs

Melis JPM, Jonker MJ, Kuiper RV, van der Hoeven TV, Robinson J, van der Horst GTJ, Breit TM, Vijg J, Dollé MET, Hoeymakers JHJ, van Steeg H.

Life-spanning murine gene expression profiles in relation to chronological and pathological aging in multiple organs

Aging Cell, Revisions, 2012

“Live, in the moment, never count on longevity”

Longevity – Yeasayer, 2012

Abstract

Aging is a complex biological process without satisfactory mechanistic explanations that accounts for a majority of observed aging effects, ranging from molecular cellular responses to organismal health deterioration and loss of homeostasis. We present a systematic *in vivo* aging study of C57BL/6J female mice, with regular sampling spanning the entire murine lifespan (13, 26, 52, 78, 104 and 130 weeks of age) from five organs for pathology and gene expression analyses. We set out to characterize aging responses in and/or between different tissues and additionally follow age-related pathways and genes in a temporal fashion throughout the lifespan. Pathological hallmarks that changed consistently during chronological aging were identified and further used to interpret biological aging, since the pathology data also revealed inter- and intra-individual variation. Aging was therefore assessed per tissue along a chronological and pathology-driven (biological) axis, correlating age-related pathological findings to gene expression profiles. Pathway analyses revealed immune responses to be commonly changed in most tissues, albeit in a tissue-specific manner. Our results furthermore indicate changes in processes that are related to imbalanced energy homeostasis, increased levels of ROS, cell cycle, cell motility and DNA damage responses. Our study enables studying temporal dynamics of genes and processes during the entire lifespan over multiple tissues, providing more insight in the temporal functional shifts that occur during aging.

Introduction

Aging is a complex process comprising a wide variety of related features and outcomes, which contribute to health deterioration with time, and eventually lead to death. Progressive functional decline, gradual deterioration of physiological function, decrease in fertility and viability and increase in vulnerability have all been related to the term aging [1].

Time and decline of physical health are the most correlated aging factors, however pinpointing specific underlying mechanisms and finding consistent aging markers is troublesome. We measured genome-wide gene expression in female C57BL/6J mice in a stringently controlled *in vivo* aging study, and incorporated time and physical health aspects in our analysis. To address the factor time, biological samples to monitor the aging process were taken systematically at regular time intervals, spanning the entire C57BL/6J lifespan. To address health and physiological deterioration, pathological and full genome expression analyses on five different organs were performed of every time point. This approach therefore permits temporal monitoring of aging during the entire lifespan ('chronological aging') and additionally can link gene expression to age-related pathology providing novel insight on 'biological aging'. Previously, numerous aging studies have provided great insight into the mechanisms that vary and play a role during aging [2-7]. However, following the temporal dynamics of proposed age-related mechanisms in a controlled setting and in multiple tissues is still troublesome. For example, the majority of microarray-based aging studies compared only two age groups (young versus old) with each other [3;8;9], or investigated model organisms with prolonged or reduced longevity [4;10]. Alternatively, *in vivo* gene expression in relation to aging has been studied using samples from a (human) population [11;12], allowing for more genetic and environmental variation. Others sampled more than three time points but have not used a full genome platform [7]. These and other large-scale meta-analyses studies [5;6] proved to be very valuable in uncovering several aging-related processes among multiple species, genotypes and tissues, but were not fit to temporally track and investigate age-related processes over the entire lifespan in multiple organs.

Previously mentioned gene expression studies revealed fairly consistent changes in the immune system and in metabolic rate during aging [3;5]. Also, several mechanisms have been postulated from previous research to at least partly explain or influence aging at the cellular level. One prevailing theory, the free radical or oxidative damage theory of aging, proposes that macromolecular damage, either due to normal toxic by-products of metabolism or inefficient repair/defensive systems, accumulates during lifespan and causes aging [13-15]. In addition, molecular pathways involving the IGF-1/GH axis [16;17] and mTOR [18;19] have also been implicated in the aging process. Nevertheless, it is still challenging to specifically indicate when, how and to what extent these molecular mechanisms affect general health deterioration and loss of homeostasis. Our study allows monitoring of these and other age-related pathways on a chronological and pathologically driven (biological) axis in multiple tissues. The latter approach additionally reveals processes that follow cellular health decline in multiple tissues.

Experimental procedures

Experimental Design

Female C57BL6/J mice were marked and randomized at the day of birth in different groups; i.e. longevity cohorts (previously described in Wijnhoven *et al.* [20]), or cross-sectional cohorts in which the mice were sacrificed at fixed time points. Cross-sectional cohorts C57BL6/J mice were sacrificed at a fixed age of 13, 26, 52, 78, 104 and 130 weeks. During the entire experiment, animals were kept in the same stringently controlled pathogen-free (spf) environment. The microbiological status of the cohorts was monitored every 3 months during the entire study. Mice were bred in-house and accommodated under pathogen-free conditions and strictly standardized day/night (12:12hr) regime at consistent temperature (20°C) and controlled air pressure. Moreover, to minimize confounding effects on health status mice were housed in small groups of 4-5 in Macrolon II type cages with sufficient cage-enrichment. Standard lab chow (Hope Farms, The Netherlands) and water were supplied ad libitum. Complete autopsy was performed on the mice; tissues were isolated from each animal and stored for further histopathological analysis (see below). Tissues were snap frozen in liquid nitrogen for gene expression profiling.

Histopathology

Organ samples of each animal were preserved in a neutral aqueous phosphate-buffered 4% solution of formaldehyde. Tissues required for microscopic examination were processed, embedded in paraffin wax, sectioned at 4 µm and stained with haematoxylin and eosin. Detailed microscopic examination was performed on 5 major organs of the mice from the interim cohort and on all gross lesions suspected of being tumors or representing major pathological conditions. For each animal, histopathological abnormalities, tumors as well as non-neoplastic lesions, were recorded and if applicable, establishing a cause of death was attempted.

The difference between the age groups of binomial data was tested using a chi-squared contingency table test. The difference between the age groups of ordinal data was tested using Kruskal-Wallis rank sum test. To determine to which extent the pathology was indicative for aging the following analysis was performed. For each pathological variable the samples were clustered on severity, using hierarchical clustering and the complete agglomeration method (with binary distance if required). The average age of the two main clusters was calculated. The allocation of each sample to either a “young” cluster or an “old” age group was afterwards compared to the chronological age of this sample to check for consistency.

Microarray analysis

Total RNA was isolated from liver, kidney, spleen, lung and brain, using the RNeasy Midi Kit (Qiagen, Valencia, CA, USA;). RNA quality was tested using automated gel electrophoresis (Bioanalyzer 2100; Agilent technologies, Amstelveen, the Netherlands (RIN > 7)). RNA samples (n = 3 per time point per tissue, 90 samples in total) were labelled and hybridized to Mouse GeneChip 430 2.0 (Affymetrix, Santa Clara, CA, USA) arrays according to the manufacturer's protocol. All raw data passed the quality criteria, but relevant effects of labelling batches were detected. The raw data from each tissue was normalized using the robust multi-array average (RMA) algorithm [21] and annotated according de

Leeuw [22]. The data were corrected for labelling-batch effects using a linear model with group-means-parametrization and coefficients for age (fixed) and labelling-batch (random). The resulting normalized expression values were analyzed for differentially expressed genes (DEGs) as described by Storey *et al.* [23], using a false discovery rate corrected p -value cut-off of < 0.05 [24]. Linear DEGs were defined based on a fitted linear regression model: each age group should have positive and negative residuals with respect to the model prediction, and average expression levels of each successive age group should change unidirectionally.

In order to discover common functionally related gene-sets in multiple tissues, the top 10% of most significantly differentially expressed genes in each tissue were tested for overrepresentation (ORA) of functionally related genes [25], using the hypergeometric test and gene-sets defined by the Gene Ontology (GO), Metacore (<http://www.genego.com/metacore.php>) and a predefined list of gene-sets (SI12). The intersection between the top 10% genes and a gene-set was called the responsive set of the gene-set. Gene-sets detected with $p < 10^{-3}$ were considered for interpretation. The profile of a gene-set was determined through the genes in the responsive set (y_i) by calculating the eigengene x [26], and the direction by $\Sigma_i \text{cor}(x, y_i)$: a negative score resulted in reversion of the eigengene. Gene-set clustering [27] was used to aid the interpretation gene-sets. ORA results were compared with the Wilcoxon rank test ($p < 10^{-5}$, gene-set analysis GSA; [28]) to examine consistency.

Co-expression was quantified using $\rho_{x,y}$ and $\rho_{x,y \cdot z}$, where ρ indicates Spearman rank correlation, x indicates a phenotypic variable, y indicates a gene and z indicates age. P-values for $\rho_{x,y}$ were determined using a permutation-based Spearman rank correlation test (ordinal data), or using a chi-squared contingency test (binomial data) and for $\rho_{x,y \cdot z}$ a conditional Spearman correlation test (ordinal data) or a Cochran-Mantel-Haenszel test (binomial data). A score for co-expression was calculated as the negative sum of the logs of the p-values of the correlation and the conditional correlation test. This methodology corrects for correlations with age. Genes in the top 3% (1000) highest co-expression scores were used for functional characterization using ORA as described above. The results were validated using GSA [28]. Gene expression data has been submitted to the public Gene Expression Omnibus, number GSE34378.

Results

Survival and intercurrent experimental setup

We have investigated six cross-sectional age groups (13, 26, 52, 78, 104 and 130 weeks of age) spanning the adult lifespan of C57BL/6J female mice. Mice were bred in-house and accommodated under specific pathogen-free (spf) conditions and strict standardized conditions. Per age group we investigated five organs (liver, kidney, spleen, lung and brain) for age-related pathology and gene expression changes. Survival and cause of death pathology could not be assessed as we sampled cross-sectional time points, but relevant information can be obtained from the concurrent longevity cohort of female mice ($n=50$, [20;29]). The most prevalent causes of death were neoplasms, inflammation and general conditional decline. To emphasize the stringent standardized conditions SI01 depicts the survival curves of the concurrent female C57BL/6J longevity study of this manuscript together with another female C57BL/6J cohort which was executed 5 years later. The comparison showed highly reproducible results, indicating these comprehensive aging studies are performed in a very

standardized and stringent setting. The percentage of animals that died per cross-sectional time point was derived from the concurrent comprehensive survival study for this manuscript: 100% of the mice in this cohort survived past the age of 52 weeks, 96% survived at 78 weeks and at 104 and 130 weeks 48% and 6% survived, respectively. The median lifespan of this cohort was 103 weeks of age and the maximum lifespan was 133 weeks (SI01).

Aging pathology in multiple tissues

The results of the pathological analyses of the six cross-sectional time points are shown in Table 1. The “Age in weeks” section of the table depicts the severity of the pathological observation represented by average scores per age group, either based on presence-absence, percentage or ordinal scoring. The last column indicates significance of the differences between the age groups. For instance, severity of karyomegaly in liver significantly increases ($p < 0.002$) with age from 3 to 5 (on an ordinal scale from 0-5). A generally accepted marker of aging at the tissue level is accumulation of lipofuscin [30]. We have scored lipofuscin accumulation during aging in a mitotic as well as a post-mitotic organ, respectively liver and brain, and found a high correlation with chronological age in both organs. Several other pathological age-related hallmarks have been scored in five tissues (Table 1). Significant aging effects were found for several parameters, but their dynamics over time vary (SI02). The most significant aging effects were found for lipofuscin accumulation in liver and brain and for glomerular membrane thickening in the kidney. Moreover, these three parameters all consistently increased over time during the entire lifespan (SI02).

Tissue	Pathology	Age in weeks						Age effect p-value
		13	26	52	78	104	130	
Liver	focal lymphoid proliferation (0-1)	33 (9)	33 (9)	17 (6)	100 (7)	80 (10)	100 (2)	0.002
	scattered extramedullary hematiopoiesis (0-5)	1 (9)	1 (9)	0 (9)	1 (10)	1 (10)	4 (3)	0.10
	karyomegaly (0-5)	3 (9)	3 (9)	3 (9)	3.5 (10)	4 (9)	5 (3)	0.002
	Intranuclear droplets (%)	0 (9)	0 (9)	0 (9)	30 (10)	89 (9)	33 (3)	0.0005
	hepatocellular vacuolization (0-5)	1 (9)	1 (8)	2 (9)	3 (10)	4 (10)	1 (3)	0.0005
	ito cell vacuolisation (0-5)	0 (9)	0 (9)	3 (8)	2 (8)	3 (7)	3 (3)	0.005
	lipofuscin index	0.63 (9)	5.44 (9)	39.40 (10)	86.63 (10)	112.4 (10)	231.1 (3)	2×10^{-7}
kidney	karyomegaly (0-5)	1 (9)	0 (9)	1 (10)	1 (10)	1 (10)	2 (3)	0.3067
	lymphoid proliferation (0-1)	0 (10)	0 (9)	56 (9)	30 (10)	40 (10)	33 (3)	0.02549
	Glomerular membrane thickening (0-5)	0 (10)	0 (8)	0 (9)	2 (10)	2.5 (10)	4 (3)	3×10^{-6}
	tubular degeneration (0-5)	0 (10)	0 (9)	0 (8)	1.5 (10)	1.5 (10)	2 (3)	0.0008
spleen	Lymphocytolysis (0-5)	3 (10)	2 (8)	1.5 (8)	1.5 (10)	0 (10)	0 (3)	0.0004
	iron laden macrophages (0-5)	0 (10)	0 (8)	2.5 (8)	3 (10)	2 (10)	1 (3)	0.005
lung	Peribronchiolar lymphoid proliferation (0-1)	10 (10)	0 (8)	50 (10)	89 (9)	89 (9)	50 (2)	0.0005
brain	vacuolisation white matter (0-5)	0 (9)	0 (7)	1 (10)	2 (10)	3 (10)	5 (3)	1×10^{-5}
	lipofuscinosis neurons HE (0-5)	0 (9)	0 (7)	0 (8)	2 (10)	2 (10)	2.5 (2)	7×10^{-6}
	periventricular GFAP* (0-4)	1 (9)	0 (6)	2 (10)	2 (10)	1 (9)	3 (3)	0.005
	hippocampus GFAP* (0-4)	1 (9)	0 (6)	2 (10)	2 (10)	2 (9)	4 (3)	0.002

*Glial Fibrillary Acidic Protein IHC staining

Table 1. Relationship between chronological aging and pathological characteristics. The pathological markers are either quantified on a continuous scale, an ordinal scale using four or five levels of severity (0-4 or 0-5), or on occurrence (absent - present). The values indicate the mean (continuous), median (ordinal) or percentage (binary) for each age class with the number of observations between brackets. The lipofuscin index in liver was calculated combining the abundance, intensity (ordinal) and size (ordinal) of lipofuscin spots. The last column indicates the significance of a difference between age classes (Age effect).

We wanted to identify the pathological hallmarks that were most likely related to biological aging. As biological and chronological aging are correlated (albeit biological variability), we hypothesized that pathological variables that are indicative for chronological age classes can potentially be related to biological aging. Figure 1A illustrates to what extent the pathology was indicative for age. For each pathological variable the samples were clustered on severity and the average age of the two main clusters was calculated (see SI03). For each individual sample, the heatmap displays whether it was allocated to the “young” group (grey = below average) or the “old” group (black = above average). Many of the variables did not yield a perfect separation between “young” and “old” in this analysis. We hypothesized that pathological variables were only indicative for aging if the two youngest cohorts (13 and 26 weeks) were assigned as “young” and the two oldest cohorts (104 and 130 weeks) were labelled as “old”. SI03 shows the percentage of correctly predicted samples for this hypothesis. Based on the best predictive values (Figure 1A and SI03), the results in Table 1 and the dynamics over time (SI02), the overall best correlating pathological parameters per tissue for chronological aging were: lipofuscin accumulation in the brain and liver, glomerular membrane thickening in the kidney, a decrease in lymphocytolysis in the spleen and increased peribronchiolar lymphoid proliferation in lung.

We also investigated if individuals showed a consistently “young” or “old” phenotype across the multiple tissues and their pathological observations and therefore systemic biological aging. Figure 1A already shows that within one animal the predicted age class can vary between and within tissues. These results indicate that there is inter- and intra-individual variation, despite the fact that some parameters give a general good indication of young and old age. The rate of biological aging was not consistently reflected in multiple pathological observations over multiple tissues, which is illustrated by Figure 1B. Here the best overall pathological parameters per tissue are depicted and four of them are shown at higher resolution than in Figure 1A. For these parameters the greyscale indicates the five levels of an ordinal scale (lymphoid proliferation in the lung was originally quantified on a binary scale). Hardly any of the individuals showed an identical ranking of greyscale for all parameters, especially in older animals.

In conclusion, several pathological hallmarks were highly correlated with chronological aging based on average scores per age group. We therefore assumed that chronological age reflected the “average ageing process” in this population. The pathology data however also indicated that there is inter- and intra-individual variation. Besides inter individual differences, aging also demonstrated to be tissue-specific within one animal. These observations let to the following strategy with respect to the gene expression analysis. We first studied gene expression profiles per tissue based on chronological age (average aging process over time). To address the biological (pathologically driven) aging, gene expression profiles were ranked for each tissue according to their co-expression with the best pathological marker for each tissue identified above.

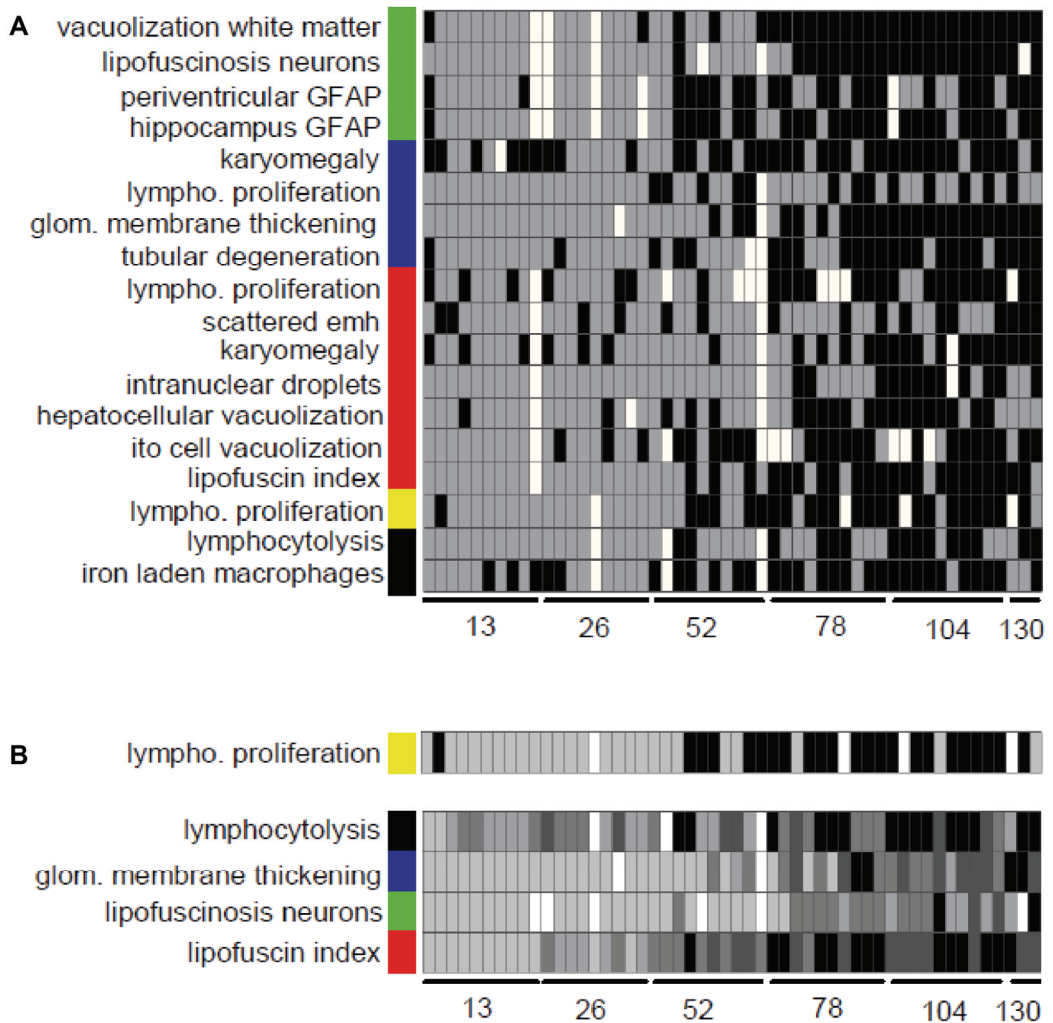


Figure 1. Heatmap indicating general age prediction (young or old) of individual samples based on the measured pathological characteristics. **(A)** Each phenotypic observation was used to cluster the samples and the average age age of the two main clusters was calculated. The heatmap indicates whether samples were part of the “young” group (grey) or the “old” group (black). White indicates missing values. The colour bar indicates tissue: brain (green), kidney (blue), liver (red), lung (yellow) and spleen (black). **(B)** The five most indicative pathological markers, of which four are shown at an ordinal scale from one (light gray) to four (black), to enable detailed comparison within individuals. Lymphoid proliferation in lung was originally measured on a binary scale, and could therefore not be transformed to the ordinal scale. White indicates missing values. The colour bar indicates tissue: brain (green), kidney (blue), liver (red), lung (yellow) and spleen (black).

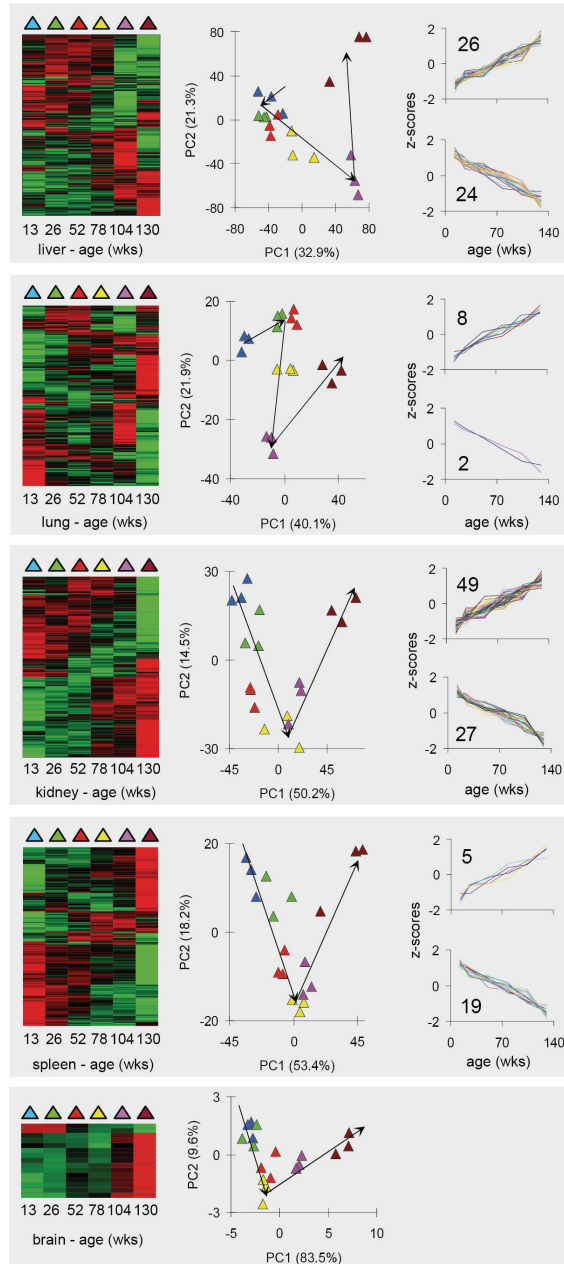


Figure 2. Age dependence of differentially expressed gene expression profiles in liver, lung, kidney, spleen and brain. The first column shows heatmaps after clustering the genes (dendrograms not shown). The second column shows scatterplots with samples plotted against the first two principal components calculated from centred and scaled expression values of the differentially expressed genes. The colours indicate age: light-blue: 13 weeks, green: 26 weeks, red: 52 weeks, yellow: 78 weeks, purple: 104 weeks and brown: 130 weeks. The last column shows graphs depicting the genes with linear expression profiles. The numbers indicate the numbers of genes.

Gene expression dynamics during chronological aging

Parallel to pathological analyses, microarray analyses were performed on all age groups in all five tissues (Figure 2). Plotting the samples against the principal components indicated that the strongest variance was explained by the differences between tissues (SI04, data not shown in this thesis). The numbers of differentially expressed genes (DEGs) based on chronological age were (FDR < 0.05): 6973 in liver tissue, 1025 in lung tissue, 2325 in kidney, 925 in spleen tissue and 15 in brain (Figure 2). All changes in expression levels of 35.283 transcripts during aging per tissue, their corresponding p-values, q-values and aging dynamics are listed in SI05 (data not shown in this thesis). Principal component analysis revealed that in general the age groups clustered, and showed a marked difference in mice of 104 and 130 weeks (Figure 2). We did not observe many transcripts with a strictly increasing or decreasing expression profile (Figure 2 and SI04). We also observed that several established age-related genes based on literature generally showed non-linear and sometimes undulating expression patterns and often revealed a tissue-specific response (SI06 depicts gene expression dynamics for *mTOR*, *p16*, *GH*, *IGF*, *PTEN*, *Sirt1*, *TGF β* , *TERT*). Emphasising the irregularity in dynamics of single genes, only a small percentage of the DEGs followed a linear expression pattern (log₂ scale, see M&M, Figure 2). Among the 6973 changing genes in the liver we found 50 DEGs with linear profiles (0.7%). In the lung, kidney and spleen we found 10, 76 and 24 DEGs with linear profiles: 1.0%, 3.3% 2.6% respectively. In summary, these analyses suggest that most age-related changes of the transcriptome are tissue-specific and the dynamics of gene expression can fluctuate greatly during the life span.

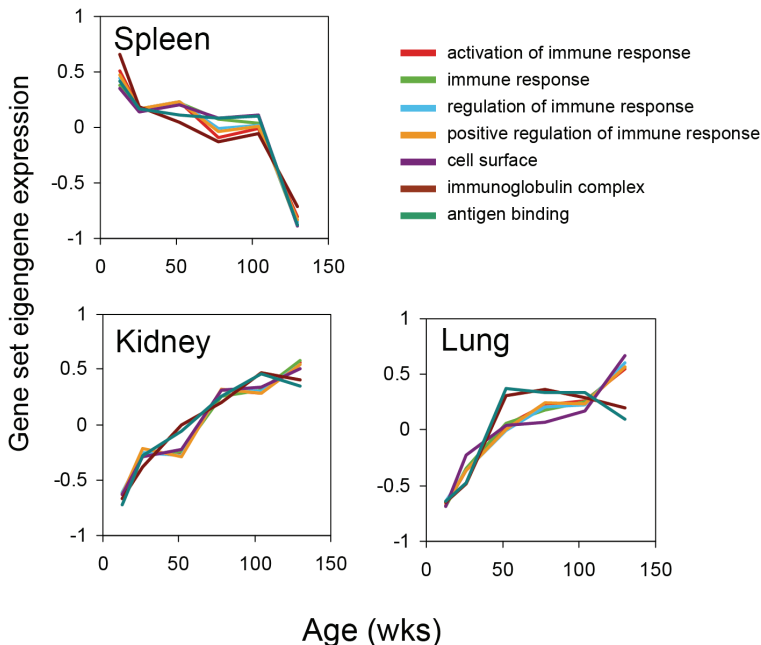


Figure 3. Tissue-specific immune-related gene-sets changes in spleen, kidney and lung. Seven gene-sets were found to have commonly changed with age in three tissues but demonstrated a tissue-specific response. The gene-sets were found through 62 responsive genes in spleen, 61 in kidney and 50 in lung. The profiles of the gene-sets, quantified using the first eigengenes of the responsive genes in the gene-sets.

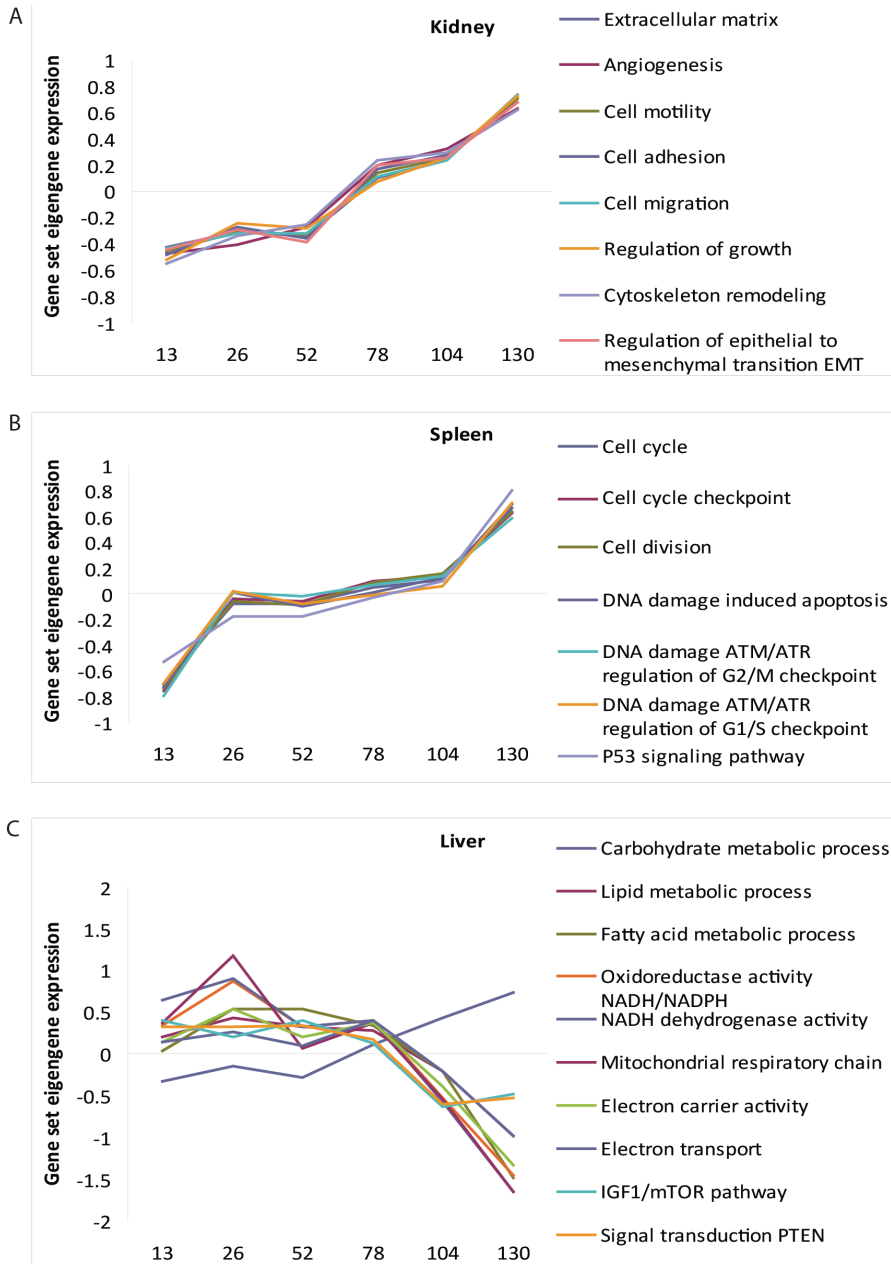


Figure 4. Dynamics of tissue-specific age-related changes. **(A)** Profiles of the gene-sets related to cell motility, migration and growth in kidney, quantified using the first eigengenes of the responsive genes in the gene-sets. **(B)** Profiles of the gene-sets related to cell cycle and DNA damage in spleen, quantified using the first eigengenes of the responsive genes in the gene-sets. **(C)** Profiles of the gene-sets related to metabolism and electron transport in liver, quantified using the first eigengenes of the responsive genes in the gene-sets.

Functional characterization of chronological age-related gene expression changes and dynamics

Next, we aimed to identify functional processes involved in aging in different tissues. We first used the Gene Ontology and overrepresentation analysis (ORA) and gene set analysis (GSA). We followed Tomlins *et al.* [25] and adopted a statistically lenient approach. The top 10% of most significant genes for each tissue were tested for overrepresentation (ORA) of functionally related genes, and the results were compared between tissues (Figure 3, 4 and detailed overview in SI07 (data not shown in this thesis)). The analyses demonstrated that most age-related changes are tissue-specific. The microarray results from brain are prone to false discoveries due to the low amount of DEGs and were therefore discarded in further analysis. Both ORA and GSA in lung, kidney and spleen indicated that the most notable gene-sets that changed during the aging process were immunological responses (Figure 3). Plotting the gene-set profiles revealed opposite directions of expression in the spleen as compared to kidney and lung, stressing a tissue-specific transcriptional response.

Besides immune response other tissue-specific, age-related changes were apparent (Figure 4). In kidney (Figure 4A), gene-sets linked to the extracellular matrix, cell motility, cell migration, angiogenesis and cell adhesion showed an age-related increase. In spleen (Figure 4B), cell cycle, cell division and DNA damage response pathways were differentially up-regulated during the lifespan.

In the liver, the majority of age-related changes in gene expression was not associated with immune response, but with metabolism and electron transport associated processes, which were mostly down-regulated (Figure 4C). Gene-set clustering on all ORA gene sets ($p \leq 0.001$) in SI07 indicated that many genes in these gene-sets were related to the mitochondrial membrane and oxidative phosphorylation (SI08). Also, PTEN and mTOR signalling pathways revealed a similar down-regulation from 78 weeks in liver (Figure 4C).

Functional pathology-related gene expression profiles

To address biological aging we focussed on the pathological variables with the best predictive values in the previous analysis: lipofuscin levels in liver or brain, thickening of the glomerular membrane in kidney, increase in peribronchiolar lymphoid proliferation in lung and the decrease in lymphocytolysis in spleen. The severity of the pathological observation was assumed to indicate the level of biological aging and all individual samples were ranked along this axis per tissue. For example, we hypothesized that a liver sample isolated from a 130 week old mouse, could biologically speaking be regarded as “younger” when the level of lipofuscin accumulation is low. A tissue sample of a 26 week old mouse with a relatively high lipofuscin level is regarded as “older”. After ranking the samples according to their biological age per tissue, we screened for genes showing co-expression with each pathological parameter. Examples of the top 10 annotated genes which are most strongly co-expressed (either positive or negative) with the biological aging parameters are shown in Figure 5. It can be seen that *Clec7a* and *Clec1b* are co-expressed with lipofuscin in liver. *Trim2* is inversely co-expressed with lymphocytolysis in spleen. Fully listed co-expression data for each tissue are fully listed in SI09 (data not shown in this thesis).

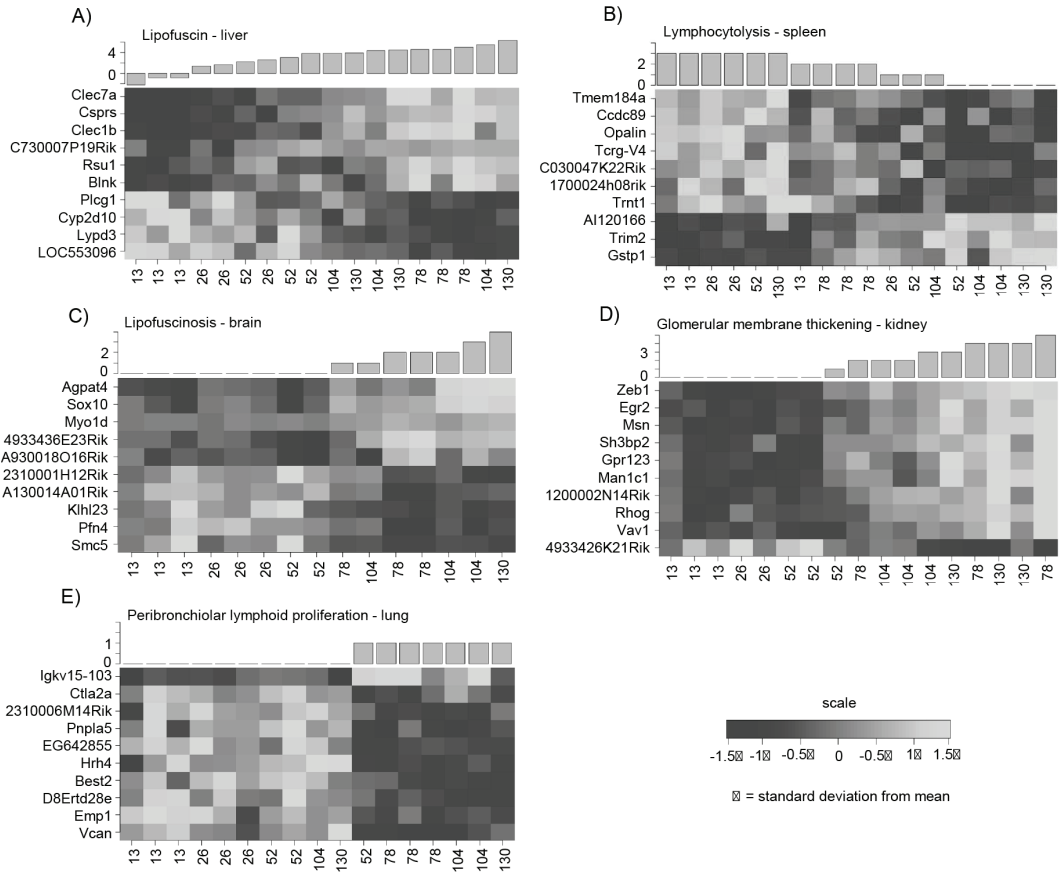


Figure 5. Biological aging biomarker per tissue. Heatmaps depicting the top 10 co-expression relationship between annotated genes and pathological aging parameters for (A) lipofuscin accumulation in the liver, (B) decrease in lymphocytolysis in the spleen, (C) lipofuscin accumulation in the brain, (D) glomerular membrane thickening in the kidney, and (E) increased peribronchiolar lymphoid proliferation in lung.

To functionally characterize pathology-driven gene expression profiles we used the same Gene Ontology and overrepresentation analysis (ORA) and gene set analysis (GSA) approaches as previously described, only now with co-expressed genes of the biological marker as input per tissue. Most of the significantly correlated gene-sets ($p < 0.0001$) found through GSA analysis were for liver lipofuscin accumulation (54 gene-sets) and kidney glomerular membrane thickening (90 gene-sets), while hardly any gene-sets were obtained for the other tissues (SI10, data not shown in this thesis). In liver, the most significantly related gene-sets indicated changes in cellular components (mostly mitochondrial (gsea)) and changes in immune response (antigen processing, presentation and binding, phagocytosis, adaptive immune response, B-cell or immunoglobulin mediated responses). In kidney, these processes were also significantly changed in correlation with biological aging. Additionally, cytoskeleton organization seemed affected, as well as cell motility, migration and adhesion (SI10). More in-depth pathway responses were further characterized in more detail per tissue using Metacore GeneGO

Pathway Maps (Table 2 and fully listed in S111). The analyses using the top 3% of most co-expressed genes per pathological parameter as input yielded a variable number of significantly regulated pathways per tissue ($p < 0.01$, FDR < 5%): Corresponding to the general results of the GSA and ORA most pathways were found for lipofuscin accumulation in liver (35) and glomerular membrane thickening in kidney (100). The other tissues showed only a small set of pathways (all results are fully listed in S111).

Pathways in liver were involved in the immune response, development, TGF-Beta-related epithelial-to-mesenchymal transition (EMT) response and Reactive Oxygen Species (ROS)-related pathways. In kidney, regulation of EMT was the most significant result and several TGF-Beta induced EMT pathways are significant. Further, cell adhesion and migration, cytoskeletal remodelling and several immune responses also appeared correlated to biological aging in the kidney. The few pathways yielded for biological aging in lung described amongst others immune response, cell cycle, cytoskeletal and cell adhesion-related pathways. The POMC processing pathway, involved in protein folding and maturation was the most significantly overrepresented pathway in lung. Lastly, in brain mostly immune-related pathways were significant, but also one DNA damage pathway, mismatch repair, is represented (Table 2 and S111).

Pathological-related functional gene expression (Metacore GeneGO Pathway Maps $p < 0.01$)		
Liver	Immune response	46% (16 from 35)
	Development	17% (6 from 35)
	ROS-related	9% (3 from 35)
	EMT-related	6% (2 from 35)
Kidney	Immune response	27% (27 from 100)
	Development	18% (18 from 100)
	Cell adhesion	12% (12 from 100)
	Cytoskeletal remodelling	12% (12 from 100)
	EMT-related	6% (6 from 100)
Lung	Cell adhesion	18% (2 from 11)
	Protein folding and maturation	9% (1 from 11)
Spleen	no significant pathways	-
Brain	Apoptosis	33% (3 from 9)
	Immune response	22% (2 from 9)
	Development	22% (2 from 9)
	DNA damage	11% (1 from 9)

Table 2. General overview of functional responses of biological aging. General overview of functional GeneGO Maps of biological (pathology-related) aging. General terms are listed in this table, detailed GeneGO Pathway Maps are fully listed in S111.

GeneGO pathway analyses revealed aging processes that were only visualized by the biological aging analyses. For example, biological aging analyses in liver (based on the pathological aging marker lipofuscin accumulation) yielded specific pathways that are related to reactive oxygen species and numerous immune-related responses. These responses were not visualized by the chronological aging

analyses. These results suggest a correlation between immune response and the level of oxidative stress during aging in liver. By combining the temporal responses during the entire lifespan and gene expression patterns linked to aging pathology our study can therefore shed some more light on the intricate processes involved in aging.

Discussion

In this comprehensive study we analysed systematic *in vivo* aging of C57BL6/J mice, based on regular samples taken during their lifespan (13, 26, 52, 78, 104 and 130 weeks of age) from five organs for pathology and gene expression analyses. We identified pathological hallmarks that are correlated with chronological aging and employed these to assess individual pathology-related (biological) aging. Besides the generally accepted aging marker lipofuscin accumulation several, potentially novel, hallmarks of aging were revealed in five different tissues (e.g. glomerular membrane thickening, lymphocytolysis in spleen and lymphoid proliferation in kidney and lung). Chronological and biological aging were functionally characterized by gene expression profiling, with the ultimate aim to confirm or find novel underlying mechanisms for aging and investigate their temporal responses during the lifespan. The combined pathological parameters in our current study demonstrated that signs of aging are predominantly tissue-specific, and the gene expression profiles confirmed this tissue-specific regulation during the course of chronological and biological aging. However, analyses based on individual genes as well as on functionally related genes gave one generally common result: the genes involved in aging commonly changing in multiple tissues were related to the immune response. The pronounced response of the immune system was also found previously in other large-scale age-related gene expression studies [^{3,5,7}]. In the comprehensive meta-analysis study of Swindell, immune responses were also the most commonly regulated processes over all tissues examined, but also biological processes like cellular respiration and other mitochondrial-related processes in liver were significantly regulated. Our study now makes it possible to monitor temporal dynamics of these and other possible age-related processes during the entire murine lifespan, which is an attractive extension for the aging field. In this study we have chosen to assess aging responses in a temporal chronological and pathology-driven (biological) manner, however, this study and accessible data also provides others with novel possibilities to address aging on a different level.

Functional characterization of the gene expression pinpointed immune responses which steadily increase or decrease with age, depending on the tissue type. Figure 3 depicted a decreasing expression of immune-related gene-sets in spleen, but an increasing expression in kidney, lung. The temporal analysis showed that the decreasing expression in spleen occurred quite sudden after 104 weeks, but increasing expression in the other tissues was more gradual. This may indicate increased immune cell infiltration upon cell death or cellular senescence in the tissues with age, but an overall decline in functionality of the immune system in spleen. The intercurrent pathological observation of lymphoid proliferation (in lung, kidney and liver) and the decrease of lymphocytolysis in spleen could partially reflect these transcriptome changes.

Our study also demonstrated that the most apparent gene expression changes observed in the liver were related to electron transport chain, metabolic processes and the mitochondrial membrane, which can reflect increasing mitochondrial and cellular dysfunction over time. The consequences of aging for mitochondria and oxidative phosphorylation have extensively been reviewed [³¹] and

decreased levels in electron transport chain have been shown in aging human tissue and other species [7]. Previous data support the finding that the rate of oxidative phosphorylation decreases during aging [32]. Our results now indicate that mitochondrial processes and oxidative phosphorylation increased moderately from very young adulthood to mature adulthood, remained constant until 78 weeks of age and then decreased considerably during the remainder of the lifespan (104 and 130 weeks). The mTOR and PTEN signaling pathways also followed this dynamic in liver. Dysregulation in both pathways has been associated with metabolic changes during aging and can also affect cancer susceptibility [33,34]. Also in other tissues we found gene expression changes that have been associated with cancer. In kidney the gene expression profiles revealed an up-regulation during aging of processes like cell motility, cell migration and angiogenesis. Several cancer associated pathways were also up-regulated in spleen: increased cell cycle and DNA damage responses were apparent, especially during the final stages of the lifespan.

Our study also showed that the pathological biomarker for ROS, lipofuscin accumulation [35], gradually increased over time, in mitotic as well as post-mitotic tissue. This supports the hypothesis that ROS and free radicals contribute to protein, lipid, RNA and DNA damage accumulation and homeostatic imbalance during aging in our study. Interestingly, the gene most strongly co-expressed with lipofuscin accumulation in liver was *Clec7a*, which is an innate immune receptor and can mediate production of ROS in the cell [36]. Also, *Hmox1* (associated with oxidative stress defense) was found to be highly correlated to lipofuscin accumulation in liver (SI09). Part of the correlated pathways to biological aging in liver revealed additional processes that were linked to ROS: e.g. TGF-beta-induction of EMT by ROS and angiotensin II-induced production of ROS (SI11). The latter pathway was also correlated to biological aging in kidney, and additionally several other EMT-related processes were notable in this tissue. Another interesting result linking lipofuscin accumulation to increased ROS was the fact that biological aging analyses in liver yielded pathways related to reactive oxygen species and numerous immune-related responses, while these responses were not identified by chronological aging analyses. These results suggest a correlation between immune response and the level of oxidative stress during aging in liver and moreover exemplify the added value of pathology-driven aging analyses. Combining temporal responses spanning the murine C57BL/6J lifespan and gene expression patterns linked to aging pathology our study provides more information on the intricate processes involved in aging.

Processes identified to be differentially regulated during aging, like mitochondrial dysfunction and the regulation of immune-related processes, are able to greatly increase ROS in cells [37,38], thereby potentially causing collateral DNA and other macromolecular damage. Since our data did not show a considerable regulation of DNA repair pathways over time or over biological aging, we expect this damage to accumulate slowly over time and influence age-related disease in most tissues, but at different rates. We have previously shown that mutations, caused by intrinsic DNA damage, increased at different rates during aging in several tissues in mice from the same intercurrent aging cohorts that were used in our current study [29]. Reversely, *in vivo* defects in DNA damage repair machinery have demonstrated to promote (segmental) accelerated aging phenotypes [20,39].

In this extensive study we analysed the process of aging on multiple levels: biological and chronological aging were assessed, combining age-related pathology and gene expression profiling. We proposed several distinguishable and potentially novel pathological hallmarks that are highly correlated to chronological aging in different tissues, but because of inter- and intra-individual variation are additionally useful to study pathology-driven, biological aging. In this study it was evident

that the immune responses played the most distinguished role in both chronological and biological aging, but manifested itself with highly tissue-specific dynamics. Our results furthermore support several aging hypotheses at the cellular level, like processes that can cause increased levels of ROS, an imbalanced metabolic or energy homeostasis or increased mutational load. Moreover, our study now enables studying temporal dynamics of genes and processes spanning the entire lifespan over multiple tissues.

Acknowledgements

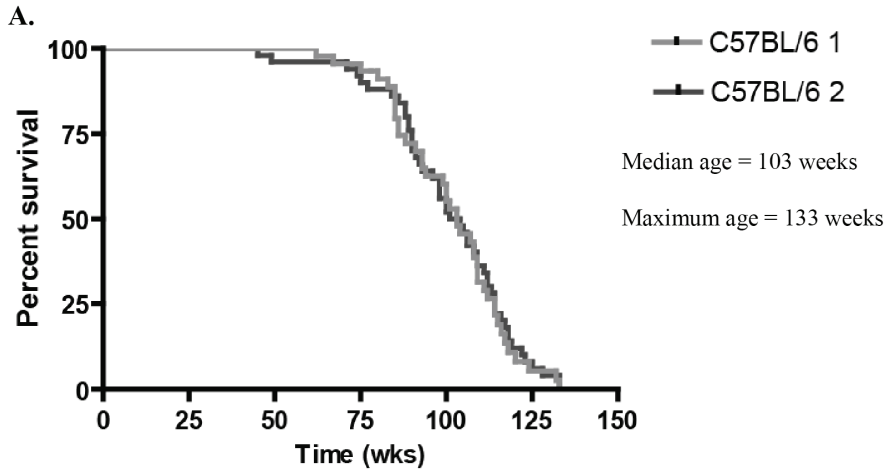
We thank the Animal Facilities of the Netherlands Vaccine Institute (NVI) for their skilful (bio)technical support. The work presented here was in part financially supported by IOP Genomics IGE03009, NIH/NIA (3PO1 AG017242), STW Grant STW-LGC.6935 and NBIC BioRange II – BR4.1. Support was also obtained from Markage (FP7-Health-2008-200880), LifeSpan (LSHG-CT-2007-036894), European Research Council (ERC advanced scientist grant JHJH).

Reference List

- [1] A.Y.Maslov, J.Vijg. Genome instability, cancer and aging, *Biochim.Biophys.Acta*, 1790, (2009) 963-969.
- [2] J.P.de Magalhaes, J.Curado, G.M.Church. Meta-analysis of age-related gene expression profiles identifies common signatures of aging, *Bioinformatics.*, 25, (2009) 875-881.
- [3] S.K.Park, K.Kim, G.P.Page, D.B.Allison, R.Weindruch, T.A.Prolla. Gene expression profiling of aging in multiple mouse strains: identification of aging biomarkers and impact of dietary antioxidants, *Aging Cell*, 8, (2009) 484-495.
- [4] W.R.Swindell. Gene expression profiling of long-lived dwarf mice: longevity-associated genes and relationships with diet, gender and aging, *BMC.Genomics*, 8, (2007) 353.
- [5] W.R.Swindell. Genes and gene expression modules associated with caloric restriction and aging in the laboratory mouse, *BMC.Genomics*, 10, (2009) 585.
- [6] W.R.Swindell, A.Johnston, L.Sun, X.Xing, G.J.Fisher, M.L.Bulyk, J.T.Elder, J.E.Gudjonsson. Meta-profiles of gene expression during aging: limited similarities between mouse and human and an unexpectedly decreased inflammatory signature, *PLoS One*, 7, (2012) e33204.
- [7] J.M.Zahn, S.Poosala, A.B.Owen, D.K.Ingram, A.Lustig, A.Carter, A.T.Weeraratna, D.D.Taub, M.Gorospe, K.Mazan-Mamczarz, E.G.Lakatta, K.R.Boheler, X.Xu, M.P.Mattson, G.Falco, M.S.Ko, D.Schlessinger, J.Firman, S.K.Kummerfeld, W.H.Wood, III, A.B.Zonderman, S.K.Kim, K.G.Becker. AGEMAP: a gene expression database for aging in mice, *PLoS Genet.*, 3, (2007) e201.
- [8] J.L.Barger, T.Kayo, J.M.Vann, E.B.Arias, J.Wang, T.A.Hacker, Y.Wang, D.Raederstorff, J.D.Morrow, C.Leeuwenburgh, D.B.Allison, K.W.Saupe, G.D.Cartee, R.Weindruch, T.A.Prolla. A low dose of dietary resveratrol partially mimics caloric restriction and retards aging parameters in mice, *PLoS.One.*, 3, (2008) e2264.
- [9] L.K.Southworth, A.B.Owen, S.K.Kim. Aging mice show a decreasing correlation of gene expression within genetic modules, *PLoS.Genet.*, 5, (2009) e1000776.
- [10] B.Schumacher, d.P.van, I, M.J.Moorhouse, T.Kosteas, A.R.Robinson, Y.Suh, T.M.Breit, H.van Steeg, L.J.Niederhofer, W.van Ijcken, A.Bartke, S.R.Spindler, J.H.Hoeijmakers, G.T.van der Horst, G.A.Garinis. Delayed and accelerated aging share common longevity assurance mechanisms, *PLoS.Genet.*, 4, (2008) e1000161.
- [11] M.L.Gron Dahl, A.C.Yding, J.Bogstad, F.C.Nielsen, H.Meinertz, R.Borup. Gene expression profiles of single human mature oocytes in relation to age, *Hum.Reprod.*, 25, (2010) 957-968.
- [12] J.M.Zahn, R.Sonu, H.Vogel, E.Crane, K.Mazan-Mamczarz, R.Rabkin, R.W.Davis, K.G.Becker, A.B.Owen, S.K.Kim. Transcriptional profiling of aging in human muscle reveals a common aging signature, *PLoS.Genet.*, 2, (2006) e115.
- [13] G.A.Garinis, G.T.van der Horst, J.Vijg, J.H.Hoeijmakers. DNA damage and ageing: new-age ideas for an age-old problem, *Nat.Cell Biol.*, 10, (2008) 1241-1247.
- [14] T.L.Parkes, A.J.Elia, D.Dickinson, A.J.Hilliker, J.P.Phillips, G.L.Boulianne. Extension of *Drosophila* lifespan by overexpression of human SOD1 in motorneurons, *Nat.Genet.*, 19, (1998) 171-174.
- [15] N.Treiber, P.Maity, K.Singh, M.Kohn, A.F.Keist, F.Ferchiu, L.Sante, S.Frese, W.Bloch, F.Kreppel, S.Kochanek, A.Sindrilaru, S.Iben, J.Hogel, M.Ohnmacht, L.E.Claes, A.Ignatius, J.H.Chung, M.J.Lee, Y.Kamenisch, M.Berneburg, T.Nikolaus, K.Braunstein, A.D.Sperfeld, A.C.Ludolph, K.Briviba, M.Wlaschek, L.Florin, P.Angel, K.Scharffetter-Kochanek. Accelerated aging phenotype in mice with conditional deficiency for mitochondrial superoxide dismutase in the connective tissue, *Aging Cell*, 10, (2011) 239-254.
- [16] G.A.Garinis, L.M.Uittenboogaard, H.Stachelscheid, M.Fousteri, W.van Ijcken, T.M.Breit, H.van Steeg, L.H.Mullenders, G.T.van der Horst, J.C.Bruning, C.M.Niessen, J.H.Hoeijmakers, B.Schumacher. Persistent transcription-blocking DNA lesions trigger somatic growth attenuation associated with longevity, *Nat.Cell Biol.*, 11, (2009) 604-615.

- [17] G.Marino, A.P.Ugalde, A.F.Fernandez, F.G.Osorio, A.Fueyo, J.M.Freije, C.Lopez-Otin. Insulin-like growth factor 1 treatment extends longevity in a mouse model of human premature aging by restoring somatotroph axis function, *Proc.Natl.Acad.Sci.U.S.A*, 107, (2010) 16268-16273.
- [18] T.Vellai, K.Takacs-Vellai, Y.Zhang, A.L.Kovacs, L.Orosz, F.Muller. Genetics: influence of TOR kinase on lifespan in *C. elegans*, *Nature*, 426, (2003) 620.
- [19] D.E.Harrison, R.Strong, Z.D.Sharp, J.F.Nelson, C.M.Astle, K.Flurkey, N.L.Nadon, J.E.Wilkinson, K.Frenkel, C.S.Carter, M.Pahor, M.A.Javors, E.Fernandez, R.A.Miller. Rapamycin fed late in life extends lifespan in genetically heterogeneous mice, *Nature*, 460, (2009) 392-395.
- [20] S.W.Wijnhoven, R.B.Beems, M.Roodbergen, B.J.van den, P.H.Lohman, K.Diderich, G.T.van der Horst, J.Vijg, J.H.Hoeijmakers, H.van Steeg. Accelerated aging pathology in ad libitum fed Xpd(ITT) mice is accompanied by features suggestive of caloric restriction, *DNA Repair (Amst)*, 4, (2005) 1314-1324.
- [21] R.A.Irizarry, B.Hobbs, F.Collin, Y.D.Beazer-Barclay, K.J.Antonellis, U.Scherf, T.P.Speed. Exploration, normalization, and summaries of high density oligonucleotide array probe level data, *Biostatistics.*, 4, (2003) 249-264.
- [22] W.C.de Leeuw, H.Rauwerda, M.J.Jonker, T.M.Breit. Salvaging Affymetrix probes after probe-level re-annotation, *BMC.Res.Notes*, 1, (2008) 66.
- [23] J.D.Storey, W.Xiao, J.T.Leeck, R.G.Tompkins, R.W.Davis. Significance analysis of time course microarray experiments, *Proc.Natl.Acad.Sci.U.S.A*, 102, (2005) 12837-12842.
- [24] J.D.Storey, R.Tibshirani. Statistical significance for genomewide studies, *Proc.Natl.Acad.Sci.U.S.A*, 100, (2003) 9440-9445.
- [25] S.A.Tomlins, R.Mehra, D.R.Rhodes, X.Cao, L.Wang, S.M.Dhanasekaran, S.Kalyana-Sundaram, J.T.Weil, M.A.Rubin, K.J.Pienta, R.B.Shah, A.M.Chinnaiyan. Integrative molecular concept modeling of prostate cancer progression, *Nat.Genet.*, 39, (2007) 41-51.
- [26] O.Alter, P.O.Brown, D.Botstein. Singular value decomposition for genome-wide expression data processing and modeling, *Proc.Natl.Acad.Sci.U.S.A*, 97, (2000) 10101-10106.
- [27] d.W.Huang, B.T.Sherman, Q.Tan, J.R.Collins, W.G.Alvord, J.Roayaei, R.Stephens, M.W.Baseler, H.C.Lane, R.A.Lempicki. The DAVID Gene Functional Classification Tool: a novel biological module-centric algorithm to functionally analyze large gene lists, *Genome Biol.*, 8, (2007) R183.
- [28] J.Michaud, K.M.Simpson, R.Escher, K.Buchet-Poyau, T.Beissbarth, C.Carmichael, M.E.Ritchie, F.Schutz, P.Cannon, M.Liu, X.Shen, Y.Ito, W.H.Raskind, M.S.Horwitz, M.Osato, D.R.Turner, T.P.Speed, M.Kavallaris, G.K.Smyth, H.S.Scott. Integrative analysis of RUNX1 downstream pathways and target genes, *BMC.Genomics*, 9, (2008) 363.
- [29] J.P.Melis, S.W.Wijnhoven, R.B.Beems, M.Roodbergen, B.J.van den, H.Moon, E.Friedberg, G.T.van der Horst, J.H.Hoeijmakers, J.Vijg, H.van Steeg. Mouse models for xeroderma pigmentosum group A and group C show divergent cancer phenotypes, *Cancer Res.*, 68, (2008) 1347-1353.
- [30] D.A.Gray, J.Woulfe. Lipofuscin and aging: a matter of toxic waste, *Sci.Aging Knowledge Environ.*, 2005, (2005) re1.
- [31] E.J.Lesnefsky, C.L.Hoppel. Oxidative phosphorylation and aging, *Ageing Res.Rev.*, 5, (2006) 402-433.
- [32] Y.Okatani, A.Wakatsuki, R.J.Reiter, Y.Miyahara. Hepatic mitochondrial dysfunction in senescence-accelerated mice: correction by long-term, orally administered physiological levels of melatonin, *J.Pineal Res.*, 33, (2002) 127-133.
- [33] R.Zoncu, A.Efeyan, D.M.Sabatini. mTOR: from growth signal integration to cancer, diabetes and ageing, *Nat.Rev.Mol.Cell Biol.*, 12, (2011) 21-35.
- [34] M.Keniry, R.Parsons. The role of PTEN signaling perturbations in cancer and in targeted therapy, *Oncogene*, 27, (2008) 5477-5485.
- [35] T.Jung, N.Bader, T.Grune. Lipofuscin: formation, distribution, and metabolic consequences, *Ann.N.Y.Acad.Sci.*, 1119, (2007) 97-111.
















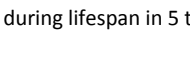


- [36] H.S.Goodridge, C.N.Reyes, C.A.Becker, T.R.Katsumoto, J.Ma, A.J.Wolf, N.Bose, A.S.Chan, A.S.Magee, M.E.Danielson, A.Weiss, J.P.Vasilakos, D.M.Underhill. Activation of the innate immune receptor Dectin-1 upon formation of a 'phagocytic synapse', *Nature*, 472, (2011) 471-475.
- [37] H.Cui, Y.Kong, H.Zhang. Oxidative stress, mitochondrial dysfunction, and aging, *J.Signal.Transduct.*, 2012, (2012) 646354.
- [38] A.P.West, I.E.Brodsky, C.Rahner, D.K.Woo, H.Erdjument-Bromage, P.Tempst, M.C.Walsh, Y.Choi, G.S.Shadel, S.Ghosh. TLR signalling augments macrophage bactericidal activity through mitochondrial ROS, *Nature*, 472, (2011) 476-480.
- [39] S.W.Wijnhoven, E.M.Hoogervorst, H.de Waard, G.T.van der Horst, H.van Steeg. Tissue specific mutagenic and carcinogenic responses in NER defective mouse models, *Mutat.Res.*, 614, (2007) 77-94.



B.

Age (weeks) Cohort 1	% survival Cohort 1	Sample size (Intercurrent study)
13	100%	10 mice
26	100%	9 mice
52	100%	10 mice
78	96%	10 mice
104	48%	10 mice
130	6%	3 mice

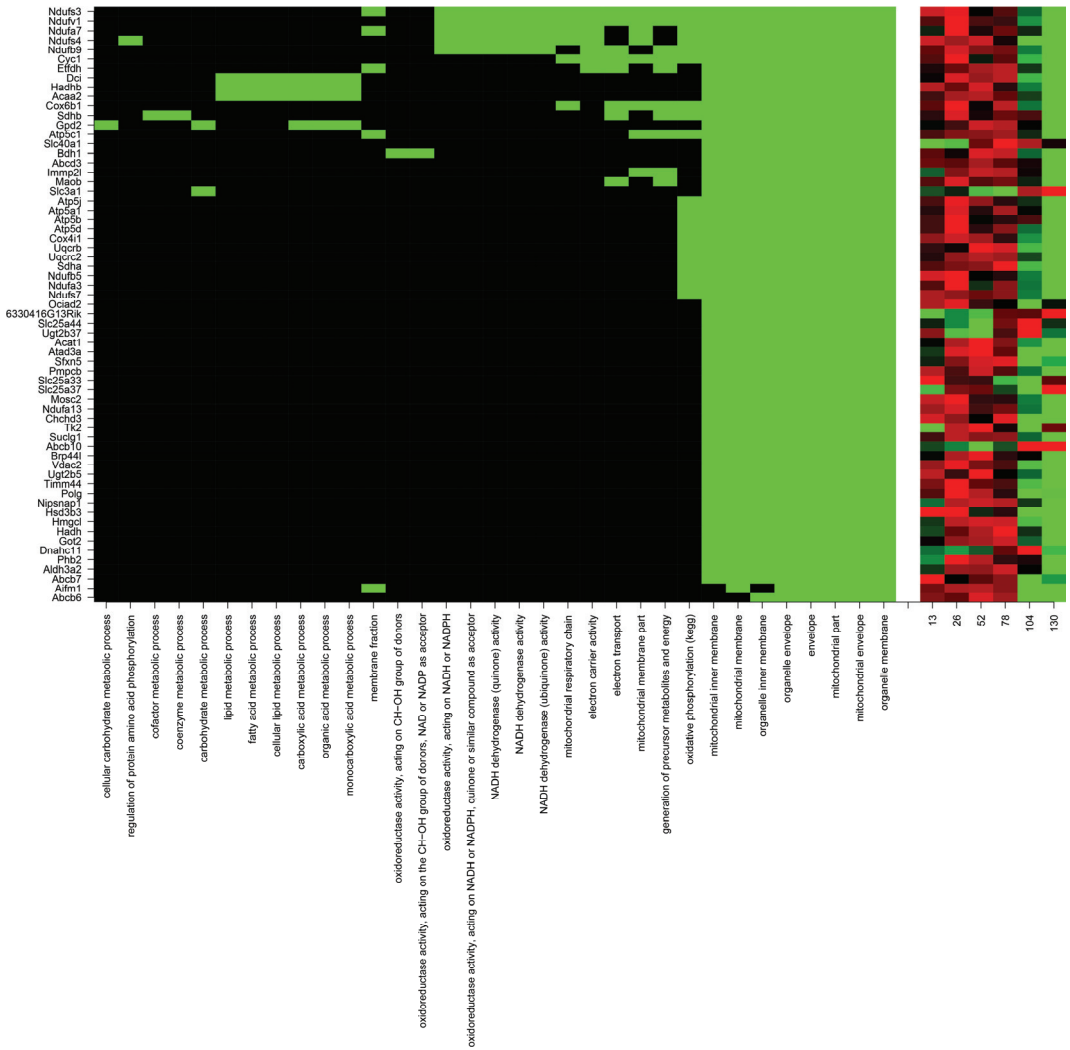
Supplemental information 1. A. Survival curves of the concurrent female wild type longevity cohort (C57BL/6J 1, $n=50$) of the study presented in this manuscript. Female cohort (C57BL/6J 2, $n=50$) was executed several years later and shows very high reproducibility. The median and maximum age for both longevity cohorts was 103 weeks and 133 weeks respectively. **B.** Overview of representative survival percentages for the intercurrent age groups used in this manuscript (deducted from cohort C57BL/6J 1). The sample size of the intercurrent age groups are also shown here. Per age group 3 samples were used for gene expression profiling and the highest number possible for pathology analysis shown in Table 1.

Tissue	Parameter	
Liver	Lymphoid proliferation	
	Scattered emh	
	Karyomegaly	
	Intranuclear droplets	
	Hepatocellular vacuolization	
	Ito cell vacuolization	
	Lipofuscin accumulation	
Kidney	Karyomegaly	
	Lymphoid proliferation	
	Glomerular membrane thickening	
	Tubular degeneration	
Spleen	Lymphocytolysis	
	Iron laden macrophages	
Lung	Peribronchiolar lymphoid proliferation	
Brain	Vacuolization white matter	
	Lipofuscin accumulation	
	Periventricular GFAP	
	Hippocampus GFAP	

Supplemental information 2. Dynamics of age-related pathological parameters during lifespan in 5 tissues

		Y	O	correct prediction young	% correct	correct prediction old	% correct
Brain	Vacuolization white matter	29.7	85.9	14/16	87.50	13/13	100.00
	Lipofuscin neurons	32.8	94.1	16/16	100.00	12/12	100.00
	Periventricular GFAP	48.4	76.8	13/15	86.67	7/12	58.33
	Hippocampus GFAP	39.0	81.6	14/15	93.33	10/12	83.33
Kidney	Karyomegaly	46.6	67.3	10/19	52.63	11/13	84.62
	Lymphoid proliferation	52.7	80.0	19/19	100.00	5/13	38.46
	Glomerular membrane thickening	32.7	92.7	18/18	100.00	13/13	100.00
	Tubular degeneration	38.0	85.3	17/19	89.47	11/13	84.62
Liver	Lymphoid proliferation	36.9	75.3	12/18	66.67	10/12	83.33
	Scattered emh	53.1	76.4	14/18	77.78	7/13	53.85
	Karyomegaly	44.0	77.4	12/18	66.67	11/12	91.67
	Intranuclear droplets	46.7	99.7	18/18	100.00	9/12	75.00
	Hepatocellular vacuolization	49.3	78.6	15/17	88.24	8/13	61.54
	Ito cell vacuolization	36.5	75.7	15/18	83.33	8/10	80.00
	Lipofuscin	38.1	89.8	18/18	100.00	11/13	84.62
	Lymphoid proliferation	35.9	80.8	17/18	94.44	9/11	81.82
Spleen	Lymphocytolysis	45.9	93.6	18/18	100.00	9/13	69.23
	Iron laden macrophages	43.6	72.1	13/18	72.22	10/13	76.92

Supplemental information 3. Predictive accuracy of each pathological parameter. The allocations of the samples to age groups indicated in Figure 1 were used to test the accuracy of the predictive age for each pathological parameter. Per age group the number of individual correct predictions were assessed where possible (absent predictions (white) were excluded from the analysis). For the young group (13 and 26 weeks) individuals should be predicted as “young” (grey) in Figure 1. For the old group (104 and 130 weeks) individuals should be predicted as “old” (black) in Figure 1. Per tissue, parameters in bold are considered most predictive and most correlated to aging. The first column (Y) indicates the average age of the samples in the young age group in weeks, the second column (O) indicates the average age of the samples in the old age group in weeks, the third column indicates the number of correct allocations to the young age group compared to the number of samples, the fourth column represents this number as a percentage, the fifth column indicates the number of correct allocations to the old age group compared to the number of samples, the sixth column represents this number as a percentage.



Supplemental information 8. Left panel: clustering analysis indicating the overlap of genes (rows) between gene-sets (columns) found in the pathways related to metabolism, oxidative phosphorylation and mitochondrial membrane. Right panel: heatmap showing the expression profiles of the genes in the gene-set-cluster across the six time points: 13, 26, 52, 78, 104 and 130 weeks.

Supplemental information 11. Complete overview of significantly regulated Metacore GeneGO Pathway Maps related to biological aging for each tissues ($p < 0.01$).

Lipofuscin accumulation - Liver

#	Maps	pValue	Ratio
1	Immune response_ Immunological synapse formation	4.608E-08	12 59
2	Immune response_ BCR pathway	1.674E-07	11 54
3	Immune response_ CCR3 signaling in eosinophils	6.724E-06	11 77
4	Immune response_ Fc epsilon RI pathway	1.528E-05	9 55
5	Immune response_ PIP3 signaling in B lymphocytes	1.229E-04	7 42
6	Immune response_ ETV3 affect on CSF1-promoted macrophage differentiation	1.607E-04	6 31
7	Immune response_ IL-5 signalling	1.666E-04	7 44
8	Development_ EPO-induced MAPK pathway	1.928E-04	7 45
9	Immune response_ Antigen presentation by MHC class II	2.251E-04	4 12
10	Oxidative stress_ Angiotensin II-induced production of ROS	3.235E-04	6 35
11	Inhibitory action of Lipoxins on Superoxide production in neutrophils	3.327E-04	7 49
12	G-protein signaling_ Rac2 regulation pathway	3.794E-04	6 36
13	Immune response_ NFAT in immune response	4.281E-04	7 51
14	Immune response_ Inhibitory action of lipoxins on superoxide production induced by IL-8 and Leukotriene B4 in neutrophils	4.281E-04	7 51
15	Immune response_ CD16 signaling in NK cells	5.422E-04	8 69
16	Blood coagulation_ GPVI-dependent platelet activation	6.842E-04	7 55
17	Chemotaxis_ Leukocyte chemotaxis	9.510E-04	8 75
18	Apoptosis and survival_ Inhibition of ROS-induced apoptosis by 17beta-estradiol	1.146E-03	6 44
19	Chemotaxis_ CCR4-induced leukocyte adhesion	1.182E-03	5 30
20	Development_ TGF-beta-induction of EMT via ROS	1.517E-03	4 19
21	Development_ TGF-beta-dependent induction of EMT via MAPK	1.629E-03	6 47
22	Development_ HGF signaling pathway	1.629E-03	6 47
23	Immune response_ IL-2 activation and signaling pathway	2.028E-03	6 49
24	Cell adhesion_ Alpha-4 integrins in cell migration and adhesion	2.113E-03	5 34
25	Chemotaxis_ Inhibitory action of lipoxins on IL-8- and Leukotriene B4-induced neutrophil migration	2.496E-03	6 51
26	Immune response_ Role of DAP12 receptors in NK cells	3.345E-03	6 54
27	Immune response_ Role of integrins in NK cells cytotoxicity	3.489E-03	5 38
28	Inhibitory action of Lipoxins on neutrophil migration	4.393E-03	6 57
29	Neurophysiological process_ Dopamine D2 receptor transactivation of PDGFR in CNS	5.038E-03	4 26
30	Regulation of lipid metabolism_ G-alpha(q) regulation of lipid metabolism	5.214E-03	6 59
31	Development_ EPO-induced PI3K/AKT pathway and Ca(2+) influx	5.993E-03	5 43
32	Development_ Angiotensin signaling via PYK2	5.993E-03	5 43
33	Immune response_ IL-15 signaling	7.754E-03	6 64
34	Immune response_ Fc gamma R-mediated phagocytosis in macrophages	8.747E-03	5 47
35	Cytoskeleton remodeling_ Reverse signaling by ephrin B	9.535E-03	4 31

Glomerular membrane thickening - Kidney

#	Maps	pValue	Ratio
1	Development_ Regulation of epithelial-to-mesenchymal transition (EMT)	7.206E-10	15 64
2	Chemotaxis_ Leukocyte chemotaxis	7.565E-09	15 75
3	Development_ Slit-Robo signaling	1.299E-08	10 30
4	Transcription_ NF-kB signaling pathway	1.741E-08	11 39
5	Cytoskeleton remodeling_ Regulation of actin cytoskeleton by Rho GTPases	2.673E-07	8 23
6	Apoptosis and survival_ Anti-apoptotic TNFs/NF-kB/IkappaB-2 pathway	3.575E-07	10 41
7	Development_ TGF-beta-dependent induction of EMT via RhoA, PI3K and ILK.	1.132E-06	10 46
8	Bacterial infections in CF airways	1.395E-06	11 58
9	Cell adhesion_ Role of tetraspanins in the integrin-mediated cell adhesion	1.434E-06	9 37
10	Immune response_ Immunological synapse formation	1.668E-06	11 59
11	Cell adhesion_ Chemokines and adhesion	2.395E-06	14 100
12	Transport_ Macropinocytosis regulation by growth factors	3.286E-06	11 63
13	Cell adhesion_ ECM remodeling	3.724E-06	10 52
14	Immune response_ CCR3 signaling in eosinophils	4.071E-06	12 77
15	Immune response_ IFN alpha/beta signaling pathway	5.904E-06	7 24
16	Cell adhesion_ Integrin inside-out signaling	7.507E-06	10 56
17	Cytoskeleton remodeling_ Neurofilaments	7.983E-06	7 25
18	Development_ TGF-beta-dependent induction of EMT via SMADs	9.260E-06	8 35
19	Chemotaxis_ Lipoxin inhibitory action on fMLP-induced neutrophil chemotaxis	9.928E-06	9 46
20	Immune response_ Oncostatin M signaling via JAK-Stat in mouse cells	1.192E-05	6 18
21	Immune response_ Fc gamma R-mediated phagocytosis in macrophages	1.195E-05	9 47
22	Immune response_ Bacterial infections in normal airways	2.023E-05	9 50
23	Cytokine production by Th17 cells in CF	2.172E-05	8 39
24	Immune response_ Oncostatin M signaling via JAK-Stat in human cells	2.361E-05	6 20
25	Apoptosis and survival_ Lymphotoxin-beta receptor signaling	3.841E-05	8 42
26	Blood coagulation_ GPVI-dependent platelet activation	4.479E-05	9 55
27	Cytoskeleton remodeling_ Keratin filaments	1.033E-04	7 36
28	Blood coagulation_ GPIIb-IX-V-dependent platelet activation	1.036E-04	10 75
29	Cytokine production by Th17 cells in CF (Mouse model)	1.215E-04	8 49
30	Cell adhesion_ Cell-matrix glycoconjugates	1.480E-04	7 38
31	Apoptosis and survival_ Anti-apoptotic TNFs/NF-kB/IAP pathway	1.500E-04	6 27
32	Chemotaxis_ Inhibitory action of lipoxins on IL-8- and Leukotriene B4-induced neutrophil migration	1.625E-04	8 51
33	Immune response_ Innate immune response to RNA viral infection	1.859E-04	6 28
34	Cytoskeleton remodeling_ Role of PKA in cytoskeleton reorganisation	2.073E-04	7 40

35	Chemotaxis_CCR4-induced leukocyte adhesion	2.780E-04	6	30
36	Immune response_TLR signaling pathways	3.167E-04	8	56
37	Blood coagulation_GPCRs in platelet aggregation	3.392E-04	9	71
38	Inhibitory action of Lipoxins on neutrophil migration	3.586E-04	8	57
39	Development_PDFG signaling via STATs and NF-κB	4.026E-04	6	32
40	Neurophysiological process_Receptor-mediated axon growth repulsion	4.416E-04	7	45
41	Role of alpha-6/beta-4 integrins in carcinoma progression	4.416E-04	7	45
42	Cell adhesion_Histamine H1 receptor signaling in the interruption of cell barrier integrity	4.416E-04	7	45
43	Development_Thrombopoietin signaling via JAK-STAT pathway	4.888E-04	5	22
44	Cell adhesion_Alpha-4 integrins in cell migration and adhesion	5.670E-04	6	34
45	Development_TGF-beta-dependent induction of EMT via MAPK	5.803E-04	7	47
46	Immune response_IL-27 signaling pathway	7.495E-04	5	24
47	Signal transduction_PKA signaling	9.605E-04	7	51
48	Immune response_Role of integrins in NK cells cytotoxicity	1.048E-03	6	38
49	Immune response_Antiviral actions of Interferons	1.081E-03	7	52
50	Cell adhesion_Cadherin-mediated cell adhesion	1.102E-03	5	26
51	Development_Cross-talk between VEGF and Angiopoietin 1 signaling pathways	1.102E-03	5	26
52	Immune response_IL-10 signaling pathway	1.102E-03	5	26
53	Development_S1P2 and S1P3 receptors in cell proliferation and differentiation	1.102E-03	5	26
54	Apoptosis and survival_APRIL and BAFF signaling	1.207E-03	6	39
55	Cytoskeleton remodeling_Cytoskeleton remodeling	1.272E-03	10	102
56	Immune response_CD16 signaling in NK cells	1.314E-03	8	69
57	Immune response_IFN gamma signaling pathway	1.357E-03	7	54
58	Immune response_MIF in innate immunity response	1.384E-03	6	40
59	Development_Delta-type opioid receptor signaling via G-protein alpha-14	1.565E-03	5	28
60	Regulation of lipid metabolism_Stimulation of Arachidonic acid production by ACM receptors	1.736E-03	8	72
61	Immune response_Neutrotenin-induced activation of IL-8 in colonocytes	1.795E-03	6	42
62	NGF activation of NF-κB	1.843E-03	5	29
63	Apoptosis and survival_TNFR1 signaling pathway	2.032E-03	6	43
64	Muscle contraction_S1P2 receptor-mediated smooth muscle contraction	2.156E-03	5	30
65	Cytoskeleton remodeling_Ra1A regulation pathway	2.156E-03	5	30
66	Cell adhesion_Gap junctions	2.156E-03	5	30
67	Cytoskeleton remodeling_TGF, WNT and cytoskeletal remodeling	2.408E-03	10	111
68	Cytoskeleton remodeling_Fibronectin-binding integrins in cell motility	2.507E-03	5	31
69	Apoptosis and survival_Role of IAP-proteins in apoptosis	2.507E-03	5	31
70	Cytoskeleton remodeling_Reverse signaling by ephrin B	2.507E-03	5	31
71	Transcription_Androgen Receptor nuclear signaling	2.577E-03	6	45
72	Immune response_ICOS pathway in T-helper cell	2.888E-03	6	46
73	Development_Transcription regulation of granulocyte development	2.896E-03	5	32
74	Development_FGF2-dependent induction of EMT	3.045E-03	4	20
75	Cell adhesion_Integrin-mediated cell adhesion and migration	3.592E-03	6	48
76	Immune response_CD40 signaling	3.988E-03	7	65
77	Cytoskeleton remodeling_Integrin outside-in signaling	3.988E-03	6	49
78	Development_EPO-induced Jak-STAT pathway	4.327E-03	5	35
79	Development_Angiopoietin - Tie2 signaling	4.327E-03	5	35
80	Oxidative stress_Angiotensin II-induced production of ROS	4.327E-03	5	35
81	Cytoskeleton remodeling_ESR1 action on cytoskeleton remodeling and cell migration	4.377E-03	4	22
82	Immune response_MIF-mediated glucocorticoid regulation	4.377E-03	4	22
83	Cytoskeleton remodeling_CDC42 in cellular processes	4.377E-03	4	22
84	Development_GM-CSF signaling	4.416E-03	6	50
85	Immune response_NFAT in immune response	4.877E-03	6	51
86	Some pathways of EMT in cancer cells	4.877E-03	6	51
87	Immune response_IL-9 signaling pathway	4.899E-03	5	36
88	Immune response_T cell receptor signaling pathway	5.372E-03	6	52
89	G-protein signaling_G-Protein alpha-12 signaling pathway	5.522E-03	5	37
90	Development_MAG-dependent inhibition of neurite outgrowth	5.522E-03	5	37
91	Development_WNT signaling pathway_Part 2	5.903E-03	6	53
92	Cell adhesion_Endothelial cell contacts by non-junctional mechanisms	6.054E-03	4	24
93	Immune response_CD28 signaling	6.471E-03	6	54
94	Immune response_Role of DAP12 receptors in NK cells	6.471E-03	6	54
95	Immune response_BCR pathway	6.471E-03	6	54
96	Translation_Regulation of EIF2 activity	6.935E-03	5	39
97	Immune response_Fc epsilon RI pathway	7.078E-03	6	55
98	Muscle contraction_Delta-type opioid receptor in smooth muscle contraction	8.111E-03	4	26
99	Cell adhesion_Endothelial cell contacts by junctional mechanisms	8.111E-03	4	26
100	Development_Role of IL-8 in angiogenesis	9.145E-03	6	58

Peribronchiolar lymphoid proliferation - Lung

#	Maps	pValue	Ratio	
1	Protein folding and maturation_POMC processing	2.924E-24	17	30
2	Immune response_IL-27 signaling pathway	2.301E-05	5	24
3	Atherosclerosis_Role of ZNF202 in regulation of expression of genes involved in Atherosclerosis	2.315E-04	4	21
4	Development_Melanocyte development and pigmentation	7.668E-04	5	49
5	Beta-alanine metabolism/ Rodent version	1.225E-03	4	32
6	Development_Angiopoietin - Tie2 signaling	1.724E-03	4	35
7	Translation_Non-genomic (rapid) action of Androgen Receptor	2.841E-03	4	40

8	Cell cycle_Chromosome condensation in prometaphase	3.536E-03	3	21
9	Cytoskeleton remodeling_Regulation of actin cytoskeleton by Rho GTPases	4.607E-03	3	23
10	Cell adhesion_ECM remodeling	7.339E-03	4	52
11	Cell adhesion_Gap junctions	9.792E-03	3	30

Lymphocytolysis - Spleen

No significant Pathway Maps

Lipofuscin accumulation - Brain

#	Maps	pValue	Ratio	
1	Development_Role of IL-8 in angiogenesis	2.591E-04	6	58
2	Regulation of lipid metabolism_Regulation of lipid metabolism via LXR, NF-Y and SREBP	2.765E-04	5	38
3	Apoptosis and survival_APRIL and BAFF signaling	3.133E-04	5	39
4	Immune response_Lectin induced complement pathway	9.168E-04	5	49
5	DNA damage_Mismatch repair	3.426E-03	3	20
6	Apoptosis and survival_Anti-apoptotic TNFs/NF-kB/Bcl-2 pathway	3.589E-03	4	41
7	Development_PEDF signaling	6.827E-03	4	49
8	Immune response_Classical complement pathway	8.419E-03	4	52
9	Apoptosis and survival_Endoplasmic reticulum stress response pathway	8.999E-03	4	53

Source	Gene set	# genes
Gene Ontology	aging_GO:0007568	24
Gene Ontology	cell_aging_GO:0007569	10
Gene Ontology	multicellular_organismal_aging_GO:0010259	7
Gene Ontology	response_to_reactive_oxygen_species_GO:0000302	16
Gene Ontology	response_to_hydrogen_peroxide_GO:0042542	10
Gene Ontology	response_to_oxygen_radical_GO:0000305	5
Gene Ontology	DNA_repair_GO:0006281	177
Gene Ontology	base-excision_repair_GO:0006284	16
Gene Ontology	double-strand_break_repair_GO:0006302	18
Gene Ontology	mismatch_repair_GO:0006298	9
Gene Ontology	non-recombinational_repair_GO:0000726	6
Gene Ontology	nucleotide-excision_repair_GO:0006289	22
Gene Ontology	recombinational_repair_GO:0000725	6
Gene Ontology	telomere_maintenance_GO:0000723	17
Gene Ontology	response_to_oxidative_stress_GO:0006979	45
Literature	Energy_restriction_and_the_GH.IGF.1_axis	13
Literature	DNA_metabolism	30
Literature	Oxidant_levels_and_redox_potential	18
Literature	Stress_response	5
BIOCARTA	ARENRF2_PATHWAY	14
BIOCARTA	INFLAM_PATHWAY	26
BIOCARTA	DEATH_PATHWAY	30
BIOCARTA	LONGEVITY_PATHWAY	15
BIOCARTA	STRESS_PATHWAY	25
BIOCARTA	WNT_PATHWAY	25
BIOCARTA	P53_PATHWAY	16
BIOCARTA	NFKB_PATHWAY	22
BIOCARTA	IGF1MTOR_PATHWAY	19
BIOCARTA	IGF1_PATHWAY	22
BIOCARTA	MTOR_PATHWAY	23
KEGG	OXIDATIVE_PHOSPHORYLATION	110
KEGG	MTOR_SIGNALING_PATHWAY	52
KEGG	BASE_EXCISION_REPAIR	30
KEGG	NUCLEOTIDE_EXCISION_REPAIR	43
KEGG	MISMATCH_REPAIR	22
KEGG	WNT_SIGNALING_PATHWAY	148
REACTOME	BASE_EXCISION_REPAIR	16
REACTOME	CELL_DEATH_SIGNALLING_VIA_NRAGE_NRIF_AND_NADE	54
REACTOME	DEATH_RECEPTOR_SIGNALLING	11
REACTOME	DNA_REPAIR	82
REACTOME	DOUBLE_STRAND_BREAK_REPAIR	19
REACTOME	EXTENSION_OF_TELOMERES	23
REACTOME	SIGNALING_BY_WNT	16
REACTOME	SYNTHESIS_OF_DNA	46
REACTOME	TELOMERE_MAINTENANCE_hs	37
REACTOME	APOPTOSIS	82
REACTOME	ENERGY_DEPENDENT_REGULATION_OF_MTOR_BY_LKB1_AMPK	12
REACTOME	MTOR_SIGNALLING	22
REACTOME	MTORC1_MEDIATED_SIGNALLING	10

Supplemental information 12. Predefined list of aging-related gene-sets based on literature

